Hearing Research 380 (2019) 100–107

Contents lists available at ScienceDirect

Hearing Research

journal homepage: www.elsevier.com/locate/heares

Research Paper

A canonical oscillator model of cochlear dynamics

Karl D. Lerud [a], Ji Chul Kim [a], Felix V. Almonte [b], Laurel H. Carney [c], Edward W. Large [a, *]

[a] Department of Psychological Sciences, University of Connecticut, Storrs, CT, USA
[b] Center for Complex Systems and Brain Sciences, Florida Atlantic University, Boca Raton, FL, USA
[c] Biomedical Engineering and Neurobiology & Anatomy, University of Rochester, Rochester, NY, USA

ARTICLE INFO

Article history:
Received 18 February 2019
Received in revised form
6 May 2019
Accepted 12 June 2019
Available online 14 June 2019

Keywords:
Cochlea
Auditory
Modeling
Dynamics
Oscillation

ABSTRACT

Nonlinear responses to acoustic signals arise through active processes in the cochlea, which has an exquisite sensitivity and wide dynamic range that can be explained by critical nonlinear oscillations of outer hair cells. Here we ask how the interaction of critical nonlinearities with the basilar membrane and other organ of Corti components could determine tuning properties of the mammalian cochlea. We propose a canonical oscillator model that captures the dynamics of the interaction between the basilar membrane and organ of Corti, using a pair of coupled oscillators for each place along the cochlea. We analyze two models in which a linear oscillator, representing basilar membrane dynamics, is coupled to a nonlinear oscillator poised at a Hopf instability. The coupling in the first model is unidirectional, and that of the second is bidirectional. Parameters are determined by fitting 496 auditory-nerve (AN) tuning curves of macaque monkeys. We find that the unidirectionally and bidirectionally coupled models account equally well for threshold tuning. In addition, however, the bidirectionally coupled model exhibits low-amplitude, spontaneous oscillation in the absence of stimulation, predicting that phase locking will occur before a significant increase in firing frequency, in accordance with well known empirical observations. This leads us to a canonical oscillator cochlear model based on the fundamental principles of critical nonlinear oscillation and coupling dynamics. The model is more biologically realistic than widely used linear or nonlinear filter-based models, yet parsimoniously displays key features of nonlinear mechanistic models. It is efficient enough for computational studies of auditory perception and auditory physiology.

© 2019 Elsevier B.V. All rights reserved.

1. Introduction

The mammalian auditory system provides the sensory functionality that allows mammals to perceive and interpret the world of sound as transmitted by air-pressure waves. The fundamental organ of this system is the cochlea. The cochlea is a detector and transducer that is sharply tuned to frequency and exquisitely sensitive, yet functions over a wide range of sound pressure levels. Along the cochlea, there is a complex interaction among the incompressible cochlear fluids and the cochlear structures including the basilar membrane (BM), sensory hair cells, supporting cells, and reticular lamina. Sound pressure-evoked BM vibrations are sensed by the outer hair cells (OHCs), which respond by producing force and oscillations (Zheng et al., 2000). The coupling between the structures of the organ of Corti (OC) through the cochlear fluids and the tectorial membrane drives the inner hair cells (IHCs), producing signals communicated to higher auditory areas by the auditory nerve (AN).

Many recent models of the cochlea focus on the nonlinear oscillatory responses of OHCs (Jülicher et al., 2001; Kern and Stoop, 2003; Magnasco, 2003; Stoop et al., 2005; Kern et al., 2008). It has been suggested that OHCs poised at or near oscillatory (Hopf) instability may be responsible for the cochlea's extreme sensitivity, excellent frequency selectivity, and amplitude compression (Camalet et al., 2000; Eguíluz et al., 2000). Models that focus on this aspect of nonlinearity in the cochlea, including the present model, are called resonance models (Bell, 2012), as distinct from transmission-line or traveling-wave models, which focus on the mechanisms underlying the traveling wave along the basilar membrane from base to apex (e.g., Neely and Rasetshwane (2017); Elliott and Ni (2018); Verhulst et al. (2018); Neely and Kim (1983)).

A novel aspect of the present oscillatory cochlear model is that it is canonical in the mathematical sense of Hoppensteadt and Izhikevich (1997a, b). Canonical model here means that a family

* Corresponding author.
E-mail address: edward.large@uconn.edu (E.W. Large).

https://doi.org/10.1016/j.heares.2019.06.001
0378-5955/© 2019 Elsevier B.V. All rights reserved.

of similar physiologically-detailed models, potentially with large numbers of parameters, can be reduced to it by a near-identity change of variables (Kim and Large, 2019). A canonical model then retains the essential properties of the highly parameterized models, while being simpler and more parsimonious. Models of OHC nonlinearities consist of dynamical equations in the form of critical oscillators that capture generic aspects of nonlinear resonance (Fredrickson-Hemsing et al., 2012; Roongthumskul et al., 2013; Hoppensteadt and Izhikevich, 1997b). Such models use the normal (truncated) form of a Hopf bifurcation

$$\dot{z} = z\left(\alpha + \mathrm{i}2\pi f + \beta|z|^2\right) + Fe^{\mathrm{i}2\pi f_0 t}, \tag{1}$$

where $z \in \mathbb{C}$ is the state variable, f is the intrinsic or natural oscillator frequency in Hz, α is a linear damping and bifurcation parameter, and β controls amplitude compression. The dot over z denotes the derivative of z with respect to time, and $Fe^{\mathrm{i}2\pi f_0 t}$ denotes linear forcing by a time-varying external signal. Because z is a complex number, it can be rewritten in polar form,

$$\dot{r} = \alpha r + \beta r^3 + F\cos(2\pi f_0 t - \phi)$$

$$\dot{\phi} = 2\pi f + \frac{F}{r}\sin(2\pi f_0 t - \phi),$$

revealing system behavior in terms of amplitude r and phase angle ϕ.

As expected for a model of oscillation, this model can exhibit resonance. Resonance means that the system oscillates at the frequency of stimulation, with amplitude and phase determined by system parameters. As the stimulus frequency f_0 approaches the intrinsic oscillator frequency f, the oscillator amplitude r increases, exhibiting bandpass filtering behavior. A canonical cochlear model in which each segment of the cochlea is represented by Eq. (1) can account for a nontrivial subset of cochlear dynamics, such as sharp mechanical frequency tuning, exquisite sensitivity, and a large dynamic range (Eguíluz et al., 2000; Magnasco, 2003; Mora and Bialek, 2011; Ospeck et al., 2001). Models of this type also lend themselves well to mathematical analysis, which is one reason for utilizing such a model in the present work. Longitudinal coupling of adjacent cochlear segments would more accurately model the traveling wave on the BM and would account for phase delays as a function of center frequency. However, including longitudinal coupling along the BM would greatly complicate the analysis, thus it was not considered in the current study.

An important question for any cochlear model is how well it represents cochlear tuning (Magnasco, 2003). Tuning curves provide information about the relationship between frequency and amplitude of the stimulus and threshold auditory responses, making tuning curves highly relevant for determining cochlear-model parameters. The cochlea is spiral-shaped and fluid-filled, making direct measurements difficult, thus most available tuning-curve data are from either the AN of laboratory animals or noninvasive measures in humans, such as psychophysical-filter bandwidth determinations or otoacoustic emissions (Shera et al., 2002). A close relationship between AN and mechanical tuning curves has been demonstrated, such that the tuning curves of fibers innervating more basal cochlear sites resemble BM tuning curves closely (Narayan et al., 1998; Temchin et al., 2008a, b). However, directly determining the mechanical-filter bandwidths in vivo in the cochlea is a difficult task, and there is not enough existing data to be especially confident in a given relationship between mechanical and neural tuning. Recent reports using optical coherence tomography suggest that mechanical tuning may be broader than initially thought (Lee et al., 2015; Dong et al., 2018); however, this technology is still being explored, and the broader tuning may simply reflect imaging a longer segment of the cochlea than intended.

Here we fit model parameters to tuning-curve data (Fig. 2) from the macaque AN (Joris et al., 2011). Starting with normal-form models of OHC nonlinearities as a theoretical framework, we introduce an extended canonical model that takes into account linear basilar-membrane dynamics, critical nonlinear OHC dynamics, and the coupling between the two. Here we study two configurations of the model. In the first model, linear basilar-membrane oscillators drive critical nonlinear OHC oscillators. In the second model, bidirectional coupling is introduced, such that the nonlinear elements reciprocally drive the linear filtering elements, in a manner similar to the model of Mountain and Hubbard (1994). Both models can be solved exactly to determine how threshold-tuning properties depend on parameters, and both models produce tuning curves that closely match responses measured in the macaque AN (Joris et al., 2011). In addition, our analysis shows that the bidirectionally coupled model produces intrinsic oscillations, such that near the empirically measured threshold there exists a bifurcation boundary between non-synchronized and synchronized physiological responses, consistent with AN phase-locking near threshold (Johnson, 1980; Köppl, 1997; Maoileidigh and Hudspeth, 2013).

2. The critical Hopf model of cochlear dynamics

Tuning curves represent a constant (isocontour) response level, or threshold, to a stimulus of particular frequency f_0 and driving force F. This response may be measured in the form of BM displacement (isodisplacement (Ruggero and Rich, 1991; Ruggero, 1992; Ruggero et al., 1992; Narayan et al., 1998),) or AN discharge rate (isorate (Narayan et al., 1998; Temchin et al., 2008a; Joris et al., 2011),). In experimental settings, the driving force F is varied until a chosen threshold response level is reached. Mathematically, the tuning curve corresponds to the intersection of a tuning surface and a plane parallel to the (f_0, F) plane passing through the threshold value of the cochlear response. The intersection is an isodisplacement or isorate contour. The tuning surface for the model defined by Eq. (1) can be determined from its polar representation by setting its amplitude equation equal to zero, i.e.,

$$\dot{r} = \alpha + \beta r^2 + \frac{F}{r}\sqrt{1 - \frac{\Omega^2 r^2}{F^2}} = 0, \tag{2}$$

where $\Omega = 2\pi(f - f_0)$. This steady-state equation involving system parameters and variables can then be solved for the desired parameter or variable. For example, the steady-state solution for r, notated as r^*, is the oscillator's steady-state amplitude. To find the tuning curve, we solved Eq. (2) for F in terms of f_0 and r^*. The resulting equation is

$$F = r^*\sqrt{\left(\alpha + \beta r^{*2}\right)^2 + \Omega^2}. \tag{3}$$

3. Fitting model parameters to tuning-curve data

To determine tuning curves that can be compared with AN data, we first passed the acoustic stimulus through a linear filter to approximate the amplitude and phase response of the middle ear (Bruce et al., 2003; Zilany and Bruce, 2006). The middle-ear filter in Zilany and Bruce (2006) is a simplified form of that of Bruce et al.

(2003). Zilany and Bruce developed a fifth-order continuous-time transfer function and represented it as a fifth-order digital filter using a bilinear transformation for a sampling frequency of 500 kHz, with the frequency axis pre-warped to give a matching frequency response at 1 kHz. To ensure stability of the digital filter, it was implemented in a second-order section form with cascading filters. The resulting waveform, denoted by $Fe^{i2\pi f_0 t}$, is provided as input to the cochlear model described in Eq. (1).

Cochlear model parameters were determined based on experimental tuning-curve data (Joris et al., 2011). A search of the parameter space revealed that even at optimal parameter values, the tuning curves produced by a model that considers only critical oscillatory dynamics are too sharp (Jülicher et al., 2001; Magnasco, 2003). Nevertheless, this model predicts several fundamental aspects of cochlear dynamics, exhibiting Hopf bifurcations controlled by the model parameter α, amplitude compression controlled by β, frequency selectivity, high sensitivity, amplification, and a wide dynamic range (Hudspeth et al., 2010). These properties are correlated with attributes of active cochlear amplification, which has been hypothesized to depend upon prestin-based electromotility of OHCs, which could increase frequency selectivity and hearing sensitivity (Dallos, 2008; Yu and Zhao, 2009).

4. Coupled canonical oscillator models

Since a single oscillator model cannot fit auditory nerve tuning-curve data well, we used pairs of coupled oscillators to model the dynamics of cochlear segments. In each pair, one oscillator represents BM displacement dynamics, and the other represents organ of Corti (OC) dynamics, including the OHCs, the tectorial membrane, and other supporting structures. Input to the complex drives the BM oscillator, which is intended to account for the dynamical effects of the pressure wave in the cochlear fluid that drives the BM. The OC energy source stems from critical oscillations that cause the organ of Corti to vibrate. Thus such a model exhibits both BM filtering and critical oscillations that capture the amplification, compression, and frequency selectivity of cochlear processing (Choe et al., 1998).

As mentioned above, this model does not include longitudinal coupling between oscillator systems and so does not capture the BM traveling wave. This also means that stimulus input is delivered to each oscillator system simultaneously. A transmission-line model that focuses on the traveling wave might include only longitudinal coupling, however both types of stimulus coupling exist in the cochlea, commonly referred to as the fast wave and slow wave (Olson, 2013; Andoh and Wada, 2004). Fast-wave coupling to the stimulus through the pressure wave in the cochlear fluid is nearly instantaneous and thus lends physiological legitimacy to this approach. Even some transmission-line models include simultaneous fast-wave coupling of the stimulus to all segments (Wit and van Dijk, 2012).

4.1. Unidirectional coupling

A model with unidirectional coupling between the pair of oscillators is more realistic than Eq. (1) in the sense that BM and OC dynamics are each represented by a model equation and coupled together to account for their respective influences on each other (cf. Jülicher et al., 2001). The natural frequency of each BM-OC complex was set to correspond to the best frequency of the cochlear segment that it represents. We equated the state of the OC oscillator with the signal that is transmitted to the AN (Narayan et al., 1998). These broad considerations led to a coupled set of canonical oscillator equations for modeling a BM-OC complex. In this model, an external stimulus drives the BM oscillator, the OC is driven by the BM, and coupling of the OC oscillator back to the BM is neglected:

$$\dot{z}_{bm} = z_{bm}(\alpha_{bm} + i2\pi f) + Fe^{i2\pi f_0 t} \tag{4}$$

$$\dot{z}_{oc} = z_{oc}\left(\alpha_{oc} + i2\pi f + (\beta + i\delta)\left|z_{oc}\right|^2\right) + c_{21} z_{bm}.$$

The state variable z_{bm} represents the dynamics of the BM, while z_{oc} represents the dynamics of the OC, including the nonlinearities of the OHCs. For simplicity, we assumed a linear BM, thus there was no nonlinear damping parameter β for the BM, and only the linear damping parameter, $\alpha_{bm} < 0$, was determined by fitting tuning-curve data. This model structure leads to bandpass filtering behavior, making the model conceptually similar to that of Jülicher et al. (2001). For the OC we assumed critical nonlinear oscillation, i.e., $\alpha_{oc} = 0$, resulting in optimal amplification (Eguíluz et al., 2000). In the general case, the nonlinear damping parameter can be complex-valued, where the real part, β, provides amplitude compression and the imaginary part δ leads to dependence of instantaneous frequency on amplitude, as has been observed in living, intact cochleae (Ruggero, 1992). However, for simplicity we assumed here that $\delta = 0$. The nonlinear damping parameter $\beta < 0$ provides amplitude compression in the OC and was also determined by fitting tuning-curve data. Finally, the parameter c_{21} governs the relative strength of forcing of the OC by the BM and was determined by fitting the data as well. The nomenclature of c_{21} follows the convention in which c_{ij} is a coefficient on the weight from the jth oscillator to the ith oscillator in a system of connected oscillators (Hoppensteadt and Izhikevich, 1997b). Thus three parameters, $\alpha_{bm} < 0$, $\beta < 0$, and $c_{21} > 0$, were determined using a search procedure that adjusted model parameters to obtain a sufficiently close match to the data, as described next.

Given an empirical tuning curve, the natural frequency f of a corresponding BM-OC oscillatory complex is set to the characteristic frequency of the AN fiber associated with the tuning curve. In order to use macaque AN threshold tuning-curve data from Joris et al. (2011) (see Fig. 2) to fit the model parameters, it is necessary for the model to be written in terms of amplitude dynamics, because our oscillator amplitude r corresponds to an fiber's firing rate. Therefore the coupled model in terms of the complex state variables z_{bm} and z_{oc}, Eq. (4), was rewritten in polar form, giving rise to amplitude and phase equations:

$$\dot{r}_{bm} = \alpha_{bm} r_{bm} + F\cos(2\pi f_0 t - \phi_{bm}) \tag{5}$$

$$\dot{\phi}_{bm} = 2\pi f + \frac{F}{r_{bm}}\sin(2\pi f_0 t - \phi_{bm})$$

$$\dot{r}_{oc} = \alpha_{oc} r_{oc} + \beta r_{oc}^3 + c_{21} r_{bm}\cos(\phi_{bm} - \phi_{oc})$$

$$\dot{\phi}_{oc} = 2\pi f + \frac{c_{21} r_{bm}}{r_{oc}}\sin(\phi_{bm} - \phi_{oc}).$$

The goal was to find the stimulus forcing amplitude F for which the oscillator z_{oc} reaches a given steady-state amplitude for a variety of stimulus frequencies. To perform a steady-state analysis for each oscillator complex we thus need to define phase-difference variables $\psi_{bm} = \phi_{bm} - 2\pi f_0 t$ and $\psi_{oc} = \phi_{oc} - \phi_{bm}$, as well as a frequency-difference parameter $\Omega = 2\pi(f - f_0)$. Adopting the notation r^*_{bm}, r^*_{oc}, ψ^*_{bm}, and ψ^*_{oc} for the steady-state amplitudes and phase differences for the oscillators, our system, which is solvable for F, becomes

$$0 = \alpha_{bm} r^*_{bm} + F\cos\psi^*_{bm} \tag{6}$$

$$0 = \Omega - \frac{F}{r^*_{bm}} \sin \psi^*_{bm}$$

$$0 = r^*_{oc}\alpha_{oc} + \beta r^{*3}_{oc} + c_{21} r^*_{bm} \cos \psi^*_{oc}$$

$$0 = \Omega + \delta r^{*2}_{oc} - \frac{c_{21} r^*_{bm}}{r^*_{oc}} \sin \psi^*_{oc}.$$

Given the threshold amplitude r^*_{oc} of z_{oc}, which is a small number that we held constant across tuning curves, the formula for F in terms of model parameters is

$$F = \frac{r^*_{oc}}{c_{21}} \left(\alpha^2_{bm} + \Omega^2\right)^{\frac{1}{2}} \left(\alpha^2_{oc} + 2r^{*2}_{oc}\alpha_{oc}\beta + r^{*4}_{oc}\beta^2 + \Omega^2 + 2\Omega\delta r^{*2}_{oc} + \delta^2 r^{*4}_{oc}\right)^{\frac{1}{2}}. \tag{7}$$

F is normally in units of pascals, which can then be converted to the stimulus level L in dB SPL by

$$L = 20 \log \frac{F}{P_0} - G, \tag{8}$$

where $P_0 = 20$ μPa represents the reference pressure, and G the gain of the middle ear filter in dB at the stimulating frequency f.

The fits assumed a threshold $r^*_{oc} = 0.1$. With the three free parameters α_{bm}, β, and c_{21} to fit for each of the 496 tuning curves in the Joris et al. (2011) data, three aspects of the model and data tuning curves were compared to minimize error and derive ideal parameters: Quality factor or Q_{ERB}, tip-to-tail difference, and absolute tip height. Q_{ERB} was determined as $\frac{CF}{ERB}$, where CF is the center frequency of the curve and the equivalent rectangular bandwidth, ERB, is determined empirically by the area under the normalized and inverted curve. The tip-to-tail (TTT) difference is a measure in decibels for how much the left side of the curve rises as the stimulating frequency decreases from CF. Because many curves in this data set did not extend a complete octave below their CF, we used a half-octave tip-to-tail measure. And tip height was simply determined as the lowest point on the curve in dB SPL, the threshold level at CF.

First, a two-parameter search was conducted for α_{bm} and β to simultaneously minimize the error for Q_{ERB} and TTT. For each data CF, an exhaustive search of α_{bm} and β combinations was used to calculate model curves. Corresponding matrices of Q_{ERB} and TTT errors were then calculated by comparing the model to the data. These error matrices were then z-scored and summed, with the lowest value of the resulting matrix determining the unique parameter regime for that CF. α_{bm} and β were therefore determined with a compromise between the errors of Q_{ERB} and TTT. Finally, to minimize the tip height error, c_{21} was calculated. To properly match the data tip heights, the model c_{21} tended to grow linearly with CF, therefore a coefficient on CF was calculated for a given curve to determine c_{21} by minimizing the error between data and model tip height in dB SPL. It is clear from Eq. (7) that c_{21} only has the effect of moving the model curve up and down, without changing its shape. Data tuning curves were compared with model tuning curves obtained in this way (Fig. 2), and raw data Q_{ERB} s, TTTs, and tip heights are shown in Fig. 4.

Solving the model for both r^*_{oc} and r^*_{bm}, compression curves can also be calculated (Fig. 3). As expected, the linear BM model approximates a Gammatone filter and does not have variable bandwidth as a function of stimulus level. Observing r^*_{oc} however, it is clear that the full unidirectional model is highly compressive, replicating the bandwidths of compression curves obtained from living, intact cochleae (Eguíluz et al., 2000; Ruggero, 1992; Ruggero et al., 1992).

It is worth noting that viewing both the data and model tuning curves in Figs. 1 and 2 in decibels obscures the fact that their Q_{ERB} s are mostly determined by the shape of the tips of the curves. Thus, the Q_{ERB} error was smaller for the lower-CF curves, and the half-octave TTT error was smaller for the higher-CF curves. While the low-frequency tails of some of the data curves often had superficially different shapes and heights than their model counterparts, it should be remembered that their filtering behavior will not be markedly different far away from CF, where both data and model require high-level stimulation relative to CF to reach threshold.

4.2. Bidirectional coupling

A more realistic configuration of the BM-OC oscillatory complexes is bidirectional coupling between the two oscillators rather than the unidirectional coupling in the previous model. Thus our second model considered the effect of OC dynamics on the BM. With bidirectional coupling, the dynamics of an oscillatory complex are governed by

$$\dot{z}_{bm} = z_{bm}(\alpha_{bm} + \mathrm{i}2\pi f) + Fe^{\mathrm{i}2\pi f_0 t} + c_{12} z_{oc} \tag{9}$$

$$\dot{z}_{oc} = z_{oc}\left(\alpha_{oc} + \mathrm{i}2\pi f + (\beta + \mathrm{i}\delta)\left|z_{oc}\right|^2\right) + c_{21} z_{bm},$$

with c_{12} being the coupling coefficient of the OC oscillator back to the BM oscillator. As was done for the unidirectional model, we derived a closed-form formula for forcing amplitude F expressed as a function of threshold amplitude r^*_{oc}, frequency difference Ω, and model parameters:

$$F = \sqrt{\left(\alpha_{bm} r^*_{bm} + c_{12} r^*_{oc} \cos \psi^*_{oc}\right)^2 + \left(\Omega r^*_{bm} + c_{12} r^*_{oc} \sin \psi^*_{oc}\right)^2} \tag{10}$$

where

$$r^*_{bm} = \frac{r^*_{oc}}{c_{21}} \sqrt{\left(\alpha_{oc} + \beta r^{*2}_{oc}\right)^2 + \left(\Omega + \delta r^{*2}_{oc}\right)^2},$$

$$\sin \psi^*_{oc} = \frac{r^*_{oc}\left(\Omega + \delta r^{*2}_{oc}\right)}{c_{21} r^*_{bm}},$$

and

$$\cos \psi^*_{oc} = \sqrt{1 - \sin^2 \psi^*_{oc}}.$$

Stability analysis of this system revealed that bidirectional coupling introduced an important change in the dynamics of BM-OC complexes. With bidirectional coupling, the two oscillators provide input to each other and as a result they have nonzero steady-state amplitudes even in the absence of external forcing. A consequence of intrinsic oscillation is that the BM-OC complex may not phase-lock to external forcing if its natural frequency is too far from the forcing frequency or if forcing is not strong enough. However, the complex may also phase lock to input before an increase in amplitude can be detected. By contrast, with unidirectional coupling and $\alpha_{oc} < 0$, both the BM and OC oscillators decay to zero when not driven by external forcing. Fig. 1, panels D–F show the resonance region or 'Arnold tongue' for a bidirectional model, within which the model phase-locks to external forcing. In general, steady-state solutions, also called fixed points, may exist outside the resonance region, but they are unstable (i.e., the model is not

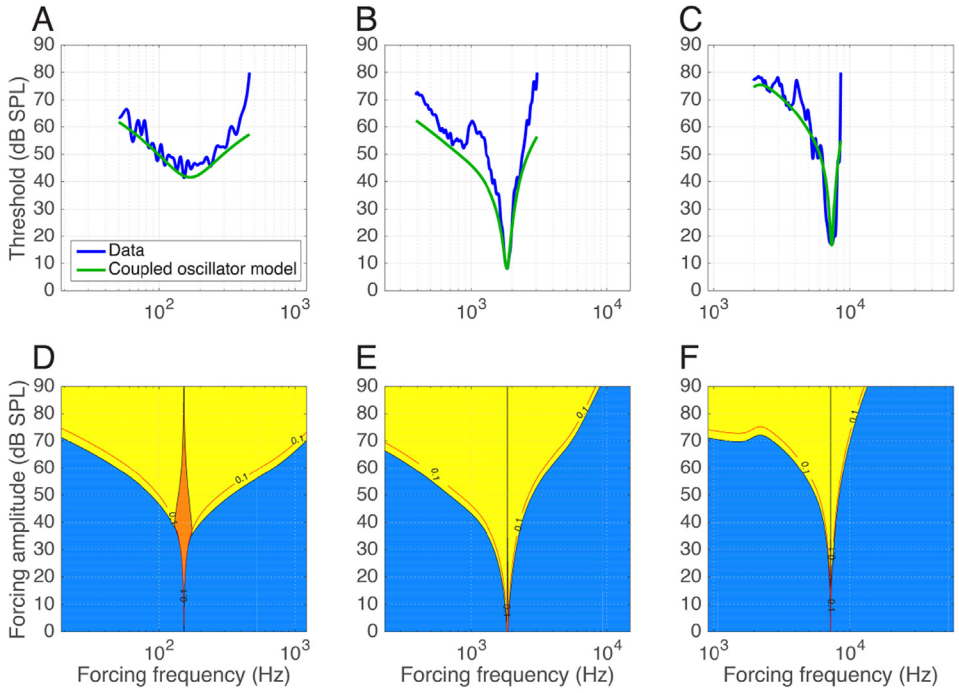

Fig. 1. Top: Fits of the unidirectionally coupled model to low (A), mid (B), and high (C) frequency AN fibers from the Joris et al. (2011) data set. Bottom: Resonance regions of the bidirectionally coupled model for low (D), mid (E), and high (F) frequency AN fibers, using the same parameters. Coupling from the OC to BM was chosen so that spontaneous amplitude was slightly below threshold amplitude, $r^*_{oc} = 0.1$. The red contours show threshold amplitude. The BM-OC model phase-locks to external forcing in the parameter regions where the fixed point is either a stable node (orange) or a stable spiral (yellow). Non-phase-locked regions (saddle points) are shown in blue. (For interpretation of the references to colour in this figure legend, the reader is referred to the Web version of this article.)

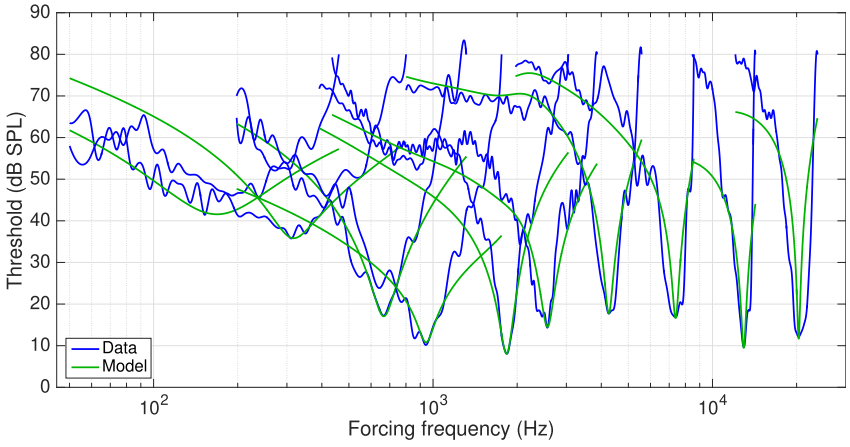

Fig. 2. Unidirectional parameter fit for ten representative tuning curves.

attracted to them). Typically, steady-state amplitudes r^*_{oc} and r^*_{bm} are unstable when they are smaller than the spontaneous amplitudes. In comparison, a BM-OC complex with unidirectional coupling and $\alpha_{oc} \leq 0$ phase-locks to external forcing of any frequency and amplitude, given enough relaxation time.

Due to the possibility of unstable solutions for bidirectional models, the forcing amplitude F obtained using Eq. (10) should be examined for its stability when the threshold amplitude r^*_{oc} is set below the spontaneous amplitude of z_{oc}. To compare tuning in this model to the tuning in the unidirectional model, we solved for the coupling parameter, c_{12}, and chose it such that spontaneous amplitude was just below threshold amplitude, $r^*_{oc} = 0.1$. Because the fitted parameters varied as a function of CF, c_{12} also did. Fig. 1 D-F shows that the tuning curves (red) lie just above the phase-locking boundary, and are similar to the tuning curves for the unidirectional model (panels A–C). Fits of the bidirectional model to the tuning-curve data did not find significant improvement over the unidirectional model. However, the bidirectional model makes the important prediction that cochlear and AN phase-locking will be observed before an increase in firing rate. This prediction matches empirical observations (Johnson, 1980; Köppl, 1997). Another important feature of this bidirectional model is spontaneous oscillation. It is well-known that many mammalian cochleae exhibit spontaneous otoacoustic emissions (Martin et al., 1988; Shera, 2003), and this aspect of auditory nonlinearity cannot be predicted with a unidirectional coupled-oscillator model.

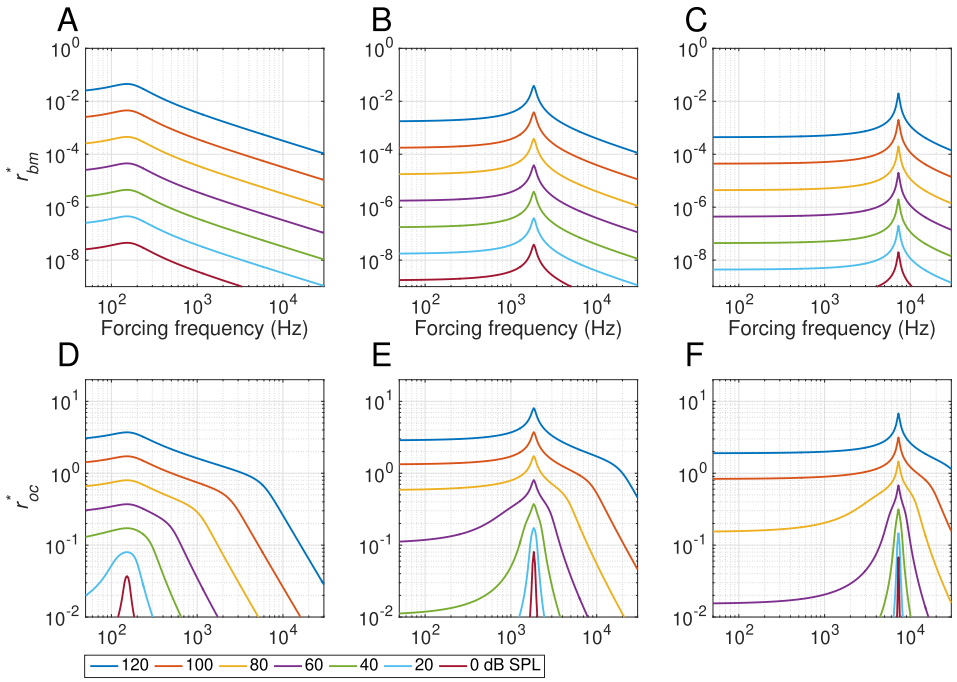

Fig. 3. Compression curves for low, mid, and high frequencies of the BM layer by itself (A–C) and of the OC layer of the unidirectionally coupled model (D–F). The BM approximates a Gammatone filterbank response alone, while the compression response of the complete model approximates compression data obtained from the cochlea itself, such as that of Ruggero (1992). Stimulus intensities are shown from 0 to 120 dB SPL in 20 dB steps.

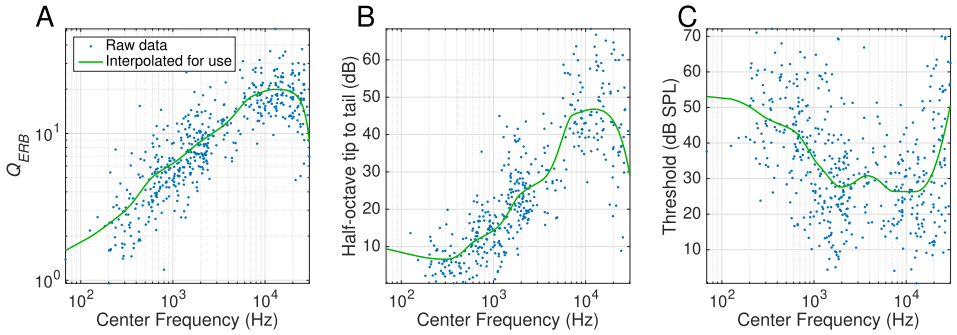

Fig. 4. Calculation of Q_{ERB} (A), half-octave tip-to-tail level difference (B), and tip level (C) from the complete Joris et al. (2011) data set. Data points are blue dots, and smoothed curves used for fitting oscillator parameters as a function of center frequency are green lines. (For interpretation of the references to colour in this figure legend, the reader is referred to the Web version of this article.)

5. Discussion

The model presented here bears some important similarities to previous work, specifically to that of Jülicher et al. (2001) and Magnasco (2003). Both of these modeling studies contained a Hopf resonance as the relevant cochlear nonlinearity, and both contained a linear filter as an input to the nonlinearity, similar to our BM model. In addition, Magnasco (2003) gives the analytical form of a tuning curve, though only for a single Hopf oscillator, similar to our Eq. (3). The present study is the first to give analytical forms for tuning curves in both unidirectional and bidirectional coupled oscillator models, where one oscillator is linear and the other operates in the critical Hopf regime. Another novel feature of this model is that stability analysis of the bidirectional parameter regime predicts spontaneous oscillation, which is known to occur in the cochlea (Kemp, 1979; Dallos, 2008). Additionally, we computed a parameter fit to AN tuning-curve data to validate the model and showed that it is much more accurate than a single critical oscillator, particularly when attempting to explain threshold tuning-curve data. Because this is a canonical model, the essence of the relevant behavior can be captured with only three parameters: α_{bm}, β, and c_{21}, with the rest chosen a priori, except c_{12} for the bidirectional model, which was calculated for each CF as described above.

The present model was validated by generating analytic threshold tuning curves and comparing their properties to macaque AN tuning curves. This method of cochlear model validation provides some unique insight into what is required of such a model, particularly of its behavior as a function of center frequency (CF). For instance, the Q_{ERB} s of the macaque tuning curves increase linearly up to approximately 5 kHz. If the curves were constant-Q, they would reflect bandwidths that vary as a function of CF, however the bandwidths below 5 kHz are roughly the same for different curves but appear narrower as CF rises on a logarithmic frequency axis (Figs. 1–2). The unidirectional model parameters we arrived at reflect this linear-Q property, as all are much less variable as a

function of frequency below 5 kHz with the exception of c_{21}. This coupling parameter between the BM and OC models varies linearly with, and correlates positively with, frequency, which may be of some physiological insight. For instance, sound first enters the cochlea at its base, where CF is highest, and travels through the spiral towards the apex, where CF is lowest. The fact that c_{21} decreases as CF decreases may reflect the dampening of the pressure wave as it travels through the fluid.

This model could be enhanced and refined in several ways. Because amplitude compression is a fundamental property of cochlear signal processing, it would be appropriate to incorporate compression data (e.g. Ruggero, 1992) to further tune the model parameters, especially the compressive nonlinearity parameter β. In addition, a number of modifications and generalizations to the model are readily possible. For instance, the assumption $\alpha_{oc} = 0$ may be relaxed, and may also improve compression curve fits. Moreover, the general nonlinear damping parameter for the Hopf model $\beta + i\delta$ is complex. For simplicity, we have kept it real in the present model, i.e. $\delta = 0$. The effect of nonzero δ would be to make instantaneous frequency dependent on amplitude, predicting a change in the resonant frequency of the cochlear segment as a function of stimulus amplitude. This phenomenon has been observed in physiological compression curves such as those in Ruggero (1992) as well as in some cochlear models such as Liu and Neely (2010). While δ would not appreciably affect threshold tuning curves, this generalization would likely improve future fits to compression curve data. The assumption of a linear BM could also be relaxed, allowing nonlinear compression in the BM and dependence of frequency on amplitude for high stimulus levels. In fact a nonlinear BM would be necessary to exploit the effects of nonzero δ because both oscillators would need nonlinear damping to properly model a cochlear segment. Finally, longitudinal coupling between adjacent cochlear oscillator systems could be introduced to increase physiological plausibility. Although this addition would render analytical forms for tuning curves impossible and analysis in general much more difficult, coupling in the apical direction between cochlear segments would more accurately simulate the effects of the BM traveling wave. The simplifying assumptions used for the present model enabled a detailed level of analysis and resulted in excellent fits to the data. Analysis of a system incorporating both a nonlinear BM and the effect of longitudinal coupling are important goals for future work.

To generate the model tuning curves shown in Fig. 2, parameters were fit to each of the 496 AN tuning curves from Joris et al. (2011), including incomplete tuning curves, highly variable tip heights, and small CF ranges. Thus, the resulting parameter values varied widely, even for curves that had nearby CFs. Therefore, to create our computational model we interpolated and extrapolated features of the empirical tuning curves to produce a single, useful set of parameter values. We smoothed the empirical Q_{ERB} s, TTTs, and tip heights by binning and interpolating (Fig. 4) and used these values to find optimal parameters for each CF from the data. The resulting model parameters were less noisy, and were themselves smoothed and interpolated to produce parameters for the computational model. The resulting model is implemented in MATLAB, and is publicly available on GitHub (Lerud et al., 2018).

In summary, we have shown that a canonical cochlear model can fit physiological data accurately with few free parameters. Because this is a nonlinear model, it cannot be computed in the frequency domain for arbitrary stimuli and must be numerically integrated, however it is more computationally tractable than models that attempt to explicitly parameterize every physical aspect of the system, and computation can be sped up through parallelization and GPU acceleration. This model is more physiologically realistic than linear filterbanks and thus it makes more accurate approximations of cochlear processing for complex signals than models such as the Gammatone filterbank. This cochlear model is well-suited for use in auditory modeling studies whose goals include modeling the perception of music and speech using physiologically realistic assumptions.

Acknowledgments

This work was supported by NSF BCS-1027761 and AFOSR FA9550-12-10388 awarded to Edward W. Large, and NIH R01-DC001641 awarded to Laurel H. Carney. The authors wish to express thanks to Philip Joris for sharing the macaque tuning-curve data, as well as thanks to Muhammad Zilany and Ian Bruce for sharing their middle ear filter coefficients.

References

Andoh, M., Wada, H., 2004. Prediction of the characteristics of two types of pressure waves in the cochlea: theoretical considerations. J. Acoust. Soc. Am. 116, 417–425. https://doi.org/10.1121/1.1763599.

Bell, A., 2012. A resonance approach to cochlear mechanics. PLoS One 7, e47918. https://doi.org/10.1371/journal.pone.0047918. URL: http://www.pubmedcentral.nih.gov/articlerender.fcgi?artid=3493581{&}tool=pmcentrez{&}rendertype=abstract.

Bruce, I.C., Sachs, M.B., Young, E.D., 2003. An auditory-periphery model of the effects of acoustic trauma on auditory nerve responses. J. Acoust. Soc. Am. 113, 369. https://doi.org/10.1121/1.1519544. http://scitation.aip.org/content/asa/journal/jasa/113/1/10.1121/1.1519544.

Camalet, S., Duke, T., Jülicher, F., Prost, J., 2000. Auditory sensitivity provided by self-tuned critical oscillations of hair cells. Proc. Natl. Acad. Sci. U. S. A. 97, 3183–3188. https://doi.org/10.1073/pnas.97.7.3183 arXiv:0003100.

Choe, Y., Magnasco, M.O., Hudspeth, A.J., 1998. A model for amplification of hair-bundle motion by cyclical binding of Ca2+ to mechanoelectrical-transduction channels. Proc. Natl. Acad. Sci. Unit. States Am. 95, 15321–15326. http://www.pnas.org/content/95/26/15321.short.

Dallos, P.J., 2008. Cochlear amplification, outer hair cells and prestin. Curr. Opin. Neurobiol. 18, 370–376. https://doi.org/10.1016/j.conb.2008.08.016 http://www.pubmedcentral.nih.gov/articlerender.fcgi?artid=2630119{&}tool=pmcentrez{&}rendertype=abstract.

Dong, W., Xia, A., Raphael, P.D., Puria, S., Applegate, B.E., Oghalai, J.S., 2018. Organ of Corti vibration within the intact gerbil cochlea measured by volumetric optical coherence tomography and vibrometry. J. Neurophysiol. 120, 2847–2857. https://doi.org/10.1152/jn.00702.2017. http://www.ncbi.nlm.nih.gov/pubmed/30281386.

Eguíluz, V.M., Ospeck, M., Choe, Y., Hudspeth, A.J., Magnasco, M.O., 2000. Essential nonlinearities in hearing. Phys. Rev. Lett. 84, 5232–5235. http://www.ncbi.nlm.nih.gov/pubmed/10990910.

Elliott, S.J., Ni, G., 2018. An elemental approach to modelling the mechanics of the cochlea. Hear. Res. 360, 14–24. https://doi.org/10.1016/j.heares.2017.10.013.

Fredrickson-Hemsing, L., Ji, S., Bruinsma, R., Bozovic, D., 2012. Mode-locking dynamics of hair cells of the inner ear. Phys. Rev. 86, 021915. https://doi.org/10.1103/PhysRevE.86.021915.

Hoppensteadt, F.C., Izhikevich, E.M., 1997a. Canonical models for mathematical neuroscience. In: Proceedings of International Conference on Neural Networks (ICNN'97), pp. 324–327. https://doi.org/10.1109/icnn.1997.611687.

Hoppensteadt, F.C., Izhikevich, E.M., 1997b. Weakly Connected Neural Networks. Springer-Verlag New York, Inc., Secaucus, NJ, USA.

Hudspeth, A.J., Jülicher, F., Martin, P., 2010. A critique of the critical cochlea: Hopf–a bifurcation–is better than none. J. Neurophysiol. 104, 1219–1229. https://doi.org/10.1152/jn.00437.2010. URL: http://www.pubmedcentral.nih.gov/articlerender.fcgi?artid=2944685{&}tool=pmcentrez{&}rendertype=abstract.

Johnson, D., 1980. The relationship between spike rate and synchrony in responses of auditory-nerve fibers to single tones. J. Acoust. Soc. Am. 68, 1115–1122. http://link.aip.org/link/?JASMAN/68/1115/1.

Joris, P.X., Bergevin, C., Kalluri, R., Mc Laughlin, M., Michelet, P., van der Heijden, M., Shera, C.A., 2011. Frequency selectivity in Old-World monkeys corroborates sharp cochlear tuning in humans. Proceedings of the National Academy of Sciences of the United States of America 108. https://doi.org/10.1073/pnas.1105867108, 17516–20. URL: http://www.pubmedcentral.nih.gov/articlerender.fcgi?artid=3198376{&}tool=pmcentrez{&}rendertype=abstract.

Jülicher, F., Andor, D., Duke, T., 2001. Physical basis of two-tone interference in hearing. Proc. Natl. Acad. Sci. U. S. A. 98 https://doi.org/10.1073/pnas.151257898, 9080–5. URL: http://www.pubmedcentral.nih.gov/articlerender.fcgi?artid=55376{&}tool=pmcentrez{&}rendertype=abstract.

Kemp, D.T., 1979. Evidence of mechanical nonlinearity and frequency selective wave amplification in the cochlea. Arch. Oto-Rhino-Laryngol. 224, 37–45. https://doi.org/10.1007/BF00455222.

Kern, A., Heid, C., Steeb, W.H., Stoop, N., Stoop, R., 2008. Biophysical parameters modification could overcome essential hearing gaps. PLoS Comput. Biol. 4, e1000161. https://doi.org/10.1371/journal.pcbi.1000161. URL: http://

www.pubmedcentral.nih.gov/articlerender.fcgi?artid=2516184{&}tool=pmcentrez{&}rendertype=abstract.
Kern, A., Stoop, R., 2003. Essential role of couplings between hearing nonlinearities. Phys. Rev. Lett. 91, 128101. https://doi.org/10.1103/PhysRevLett.91.128101. http://link.aps.org/doi/10.1103/PhysRevLett.91.128101.
Kim, J.C., Large, E.W., 2019. Mode locking in periodically forced gradient frequency neural networks. Phys. Rev. 99, 1–11. https://doi.org/10.1103/PhysRevE.99.022421.
Köppl, C., 1997. Phase locking to high frequencies in the auditory nerve and cochlear nucleus magnocellularis of the barn owl, Tyto alba. J. Neurosci. 17, 3312–3321. http://www.ncbi.nlm.nih.gov/pubmed/9096164.
Lee, H.Y., Raphael, P.D., Park, J., Ellerbee, A.K., Applegate, B.E., Oghalai, J.S., 2015. Noninvasive in vivo imaging reveals differences between tectorial membrane and basilar membrane traveling waves in the mouse cochlea. Proc. Natl. Acad. Sci. Unit. States Am. 112, 3128–3133. https://doi.org/10.1073/pnas.1500038112.
Lerud, K.D., Kim, J.C., Large, E.W., 2018. https://github.com/MusicDynamicsLab/GrFNNCochlea. URL: https://github.com/MusicDynamicsLab/GrFNNCochlea.
Liu, Y.W., Neely, S.T., 2010. Distortion product emissions from a cochlear model with nonlinear mechanoelectrical transduction in outer hair cells. J. Acoust. Soc. Am. 127, 2420–2432. https://doi.org/10.1121/1.3337233.
Magnasco, M., 2003. A wave traveling over a Hopf instability shapes the cochlear tuning curve. Phys. Rev. Lett. 90, 058101. https://doi.org/10.1103/PhysRevLett.90.058101.
Maoileidigh, D.O., Hudspeth, A.J., 2013. Effects of cochlear loading on the motility of active outer hair cells. Proc. Natl. Acad. Sci. Unit. States Am. 110, 5474–5479. https://doi.org/10.1073/pnas.1302911110.
Martin, G.K., Lonsbury-Martin, B.L., Probst, R., Coats, A.C., 1988. Spontaneous otoacoustic emissions in a nonhuman primate. I. Basic features and relations to other emissions. Hear. Res. 33, 49–68. http://www.ncbi.nlm.nih.gov/pubmed/3372370.
Mora, T., Bialek, W., 2011. Are biological systems poised at criticality? J. Stat. Phys. 144, 268–302. https://doi.org/10.1007/s10955-011-0229-4.
Mountain, D.C., Hubbard, A.E., 1994. A piezoelectric model of outer hair cell function. J. Acoust. Soc. Am. 95, 350–354. https://doi.org/10.1121/1.408273. http://www.ncbi.nlm.nih.gov/pubmed/8120246.
Narayan, S.S., Temchin, A.N., Recio, A., Ruggero, M.A., 1998. Frequency tuning of basilar membrane and auditory nerve fibers in the same cochleae. Science (New York, N.Y.) 282, 1882–1884. https://doi.org/10.1126/science.282.5395.1882.
Neely, S.T., Kim, D.O., 1983. An active cochlear model showing sharp tuning and high sensitivity. Hear. Res. 9, 123–130. https://doi.org/10.1016/0378-5955(83)90022-9.
Neely, S.T., Rasetshwane, D.M., 2017. Modeling signal propagation in the human cochlea. J. Acoust. Soc. Am. 142, 2155–2167. https://doi.org/10.1121/1.5007719.
Olson, E.S., 2013. Fast waves, slow waves and cochlear excitation. J. Acoust. Soc. Am. 133, 3508. https://doi.org/10.1121/1.4806254, 3508. https://doi.org/10.1121/1.4799326.
Ospeck, M., Eguíluz, V.M., Magnasco, M., 2001. Evidence of a Hopf bifurcation in frog hair cells. Biophys. J. 80, 2597–2607. http://www.sciencedirect.com/science/article/pii/S0006349501762303.
Roongthumskul, Y., Shlomovitz, R., Bruinsma, R., Bozovic, D., 2013. Phase slips in oscillatory hair bundles. Phys. Rev. Lett. 110, 148103. https://doi.org/10.1103/PhysRevLett.110.148103.
Ruggero, M.A., 1992. Responses to sound of the basilar membrane of the mammalian of cochlea. Curr. Opin. Neurobiol. 2, 449–456. http://www.sciencedirect.com/science/article/pii/095943889290179O.
Ruggero, M.A., Rich, N.C., 1991. Application of a commercially-manufactured Doppler-shift laser velocimeter to the measurement of basilar-membrane vibration. Hear. Res. 51, 215–230. https://doi.org/10.1016/0378-5955(91)90038-B.
Ruggero, M.A., Robles, L., Rich, N.C., Recio, A., 1992. Basilar membrane responses to two-tone and broadband stimuli. Philos. Trans. R. Soc. Lond. Ser. B Biol. Sci. 336, 307–314. https://doi.org/10.1098/rstb.1992.0063 discussion 314–5. URL: http://www.pubmedcentral.nih.gov/articlerender.fcgi?artid=3578387{&}tool=pmcentrez{&}rendertype=abstract.
Shera, C.A., 2003. Mammalian spontaneous otoacoustic emissions are amplitude-stabilized cochlear standing waves. J. Acoust. Soc. Am. 114, 244–262. https://doi.org/10.1121/1.1575750.
Shera, C.A., Guinan, J.J., Oxenham, A.J., 2002. Revised estimates of human cochlear tuning from otoacoustic and behavioral measurements. Proc. Natl. Acad. Sci. U. S. A. 99, 3318–3323. https://doi.org/10.1073/pnas.032675099. URL: http://www.pubmedcentral.nih.gov/articlerender.fcgi?artid=122516{&}tool=pmcentrez{&}rendertype=abstract.
Stoop, R., Steeb, W.H., Gallas, J., Kern, A., 2005. Auditory two-tone suppression from a subcritical Hopf cochlea. Phys. Stat. Mech. Appl. 351, 175–183. https://doi.org/10.1016/j.physa.2004.12.019. URL: http://linkinghub.elsevier.com/retrieve/pii/S0378437104015626.
Temchin, A.N., Rich, N.C., Ruggero, M.A., 2008a. Threshold tuning curves of chinchilla auditory-nerve fibers. I. Dependence on characteristic frequency and relation to the magnitudes of cochlear vibrations. J. Neurophysiol. 100, 2889–2898. https://doi.org/10.1152/jn.90637.2008. URL: http://www.pubmedcentral.nih.gov/articlerender.fcgi?artid=2585409{&}tool=pmcentrez{&}rendertype=abstract.
Temchin, A.N., Rich, N.C., Ruggero, M.A., 2008b. Threshold tuning curves of chinchilla auditory nerve fibers. II. Dependence on spontaneous activity and relation to cochlear nonlinearity. J. Neurophysiol. 100, 2899–2906. https://doi.org/10.1152/jn.90639.2008. URL: http://www.pubmedcentral.nih.gov/articlerender.fcgi?artid=2585395{&}tool=pmcentrez{&}rendertype=abstract.
Verhulst, S., Altoè, A., Vasilkov, V., 2018. Computational modeling of the human auditory periphery: auditory-nerve responses, evoked potentials and hearing loss. Hear. Res. 360, 55–75. https://doi.org/10.1016/j.heares.2017.12.018.
Wit, H.P., van Dijk, P., 2012. Are human spontaneous otoacoustic emissions generated by a chain of coupled nonlinear oscillators? J. Acoust. Soc. Am. 132, 918–926. https://doi.org/10.1121/1.4730886.
Yu, N., Zhao, H.B., 2009. Modulation of outer hair cell electromotility by cochlear supporting cells and gap junctions. PLoS One 4, e7923. https://doi.org/10.1371/journal.pone.0007923. URL: http://www.pubmedcentral.nih.gov/articlerender.fcgi?artid=2775161{&}tool=pmcentrez{&}rendertype=abstract.
Zheng, J., Shen, W., He, D.Z., Long, K.B., Madison, L.D., Dallos, P.J., 2000. Prestin is the motor protein of cochlear outer hair cells. Nature 405, 149–155. https://doi.org/10.1038/35012009. URL: http://www.ncbi.nlm.nih.gov/pubmed/10821263.
Zilany, M.S.A., Bruce, I.C., 2006. Modeling auditory-nerve responses for high sound pressure levels in the normal and impaired auditory periphery. J. Acoust. Soc. Am. 120, 1446. https://doi.org/10.1121/1.2225512. URL: http://scitation.aip.org/content/asa/journal/jasa/120/3/10.1121/1.2225512.